ACS APPLIED MATERIALS & INTERFACES

Research Article

www.acsami.org

Electrospun Three-Dimensional Mesoporous Silicon Nanofibers as an Anode Material for High-Performance Lithium Secondary Batteries

Dong Jin Lee,[†] Hongkyung Lee,[†] Myung-Hyun Ryou,[‡] Gi-Beom Han,[§] Je-Nam Lee,[†] Jongchan Song,[†] Jaecheol Choi,[‡] Kuk Young Cho,[⊥] Yong Min Lee,*[,‡] and Jung-Ki Park*[,†]

[†]Department of Chemical and Biomolecular Engineering, Korea Advanced Institute of Science and Technology (KAIST), Daejeon 305-701, Republic of Korea

[‡]Department of Chemical and Biological Engineering, Hanbat National University, Daejeon 305-719, Republic of Korea

[§]Battery R & D, LG Chem, Ltd., 104-1 Moonji dong, Yuseong-gu, Daejeon 305-380, Republic of Korea

[⊥]Division of Advanced Materials Engineering, Kongju National University, Cheonan-daero, Seobuk-gu, Cheonan, Chungnam 331-717, Republic of Korea

Supporting Information

ABSTRACT: Mesoporous silicon nanofibers (m-SiNFs) have been fabricated using a simple and scalable method via electrospinning and reduction with magnesium. The prepared m-SiNFs have a unique structure in which clusters of the primary Si nanoparticles interconnect to form a secondary three-dimensional mesoporous structure. Although only a few nanosized primary Si particles lead to faster electronic and Li^+ ion diffusion compared to tens of nanosized Si, the secondary nanofiber structure (a few micrometers in length) results in the uniform distribution of the nanoparticles, allowing for the easy fabrication of electrodes. Moreover, these m-SiNFs exhibit impressive electrochemical characteristics when used as the anode materials in lithium ion batteries (LIBs). These include a high reversible capacity of 2846.7 mAh g^{-1} at a current density of 0.1 A g^{-1}, a stable capacity retention of 89.4% at a 1 C rate (2 A g^{-1}) for 100 cycles, and a rate capability of 1214.0 mAh g^{-1} (at 18 C rate for a discharge time of ~3 min).

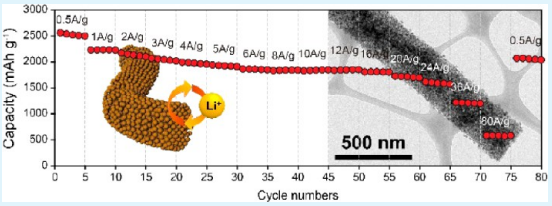

KEYWORDS: *silicon anode, porous silicon structure, electrospinning, magnesiothermic reduction, silicon nanofiber*

1. INTRODUCTION

For over a decade, lithium ion batteries (LIBs) have been the preferred source of electric power for mobile devices such as digital cameras, smart phones, and laptop computers. This is owing to their high energy density per volume (volumetric) and weight (gravimetric).[1−3] However, the depletion of petroleum resources coupled with regulations to reduce environmental pollution has created a new demand for large-scale LIBs for electrical vehicles (EVs)[4,5] and for sustainable energy storage systems (ESSs) to store energy from renewable sources (water, sun, biomass, geothermal, and hydrogen).[6] These large-scale LIBs should ideally exhibit a variety of reversible capacities, cyclabilities, and power capabilities to meet this demand.[7−9]

Graphitic carbon has been widely used as a commercial anode material because of its high coulombic efficiency and superior cyclability.[10,11] However, owing to its relatively low theoretical capacity (372 mAh g^{-1}), significant efforts have been dedicated to finding high-capacity anode materials that exhibit high efficiencies and long-term stability.[12−14] Among the various candidate materials, Si has been investigated extensively because of its extremely high theoretical capacity (4200 mAh g^{-1}).[15−17] Nevertheless, the practical use of Si anodes is hindered by the fact that the Si particles in the anodes undergo pulverization accompanied by large volume changes (up to 300%) during cycling, resulting in electrically isolated and dead Si anodes. This is accompanied by the continuous growth of a solid electrolyte interphase (SEI) layer on the newly exposed surfaces of the Si anodes owing to electrolyte decomposition.[15,18,19] Various nanosized or nanostructured Si materials, whose electrochemical performances are significantly better than those of micrometer-sized Si materials,[20] have been proposed to address this problem.[17,21−23] In particular, nanoscaled Si structures such as nanowires,[21] hollow nanoparticles,[22] and nanotubes[23] can efficiently accommodate the large strains and stresses that result from the Li−Si alloying reaction. However, their synthesis methods have inherent limitations, which prevent the commercial use of the thus-synthesized Si anodes. For example, these processes are complex and have low yields, and the synthesized anodes exhibit low volumetric capacities owing to their packing densities being low.[24,25]

Bao et al. employed a reduction process involving the use of a silica template to produce porous Si.[26] Although various previous studies have demonstrated mesoporous Si nanoparticles,[27] hollow Si nanospheres,[28] Si nanotubes,[29] and Si nanowires[30] via the same process showing reliable electro-

Received: September 4, 2013
Accepted: November 6, 2013
Published: November 6, 2013

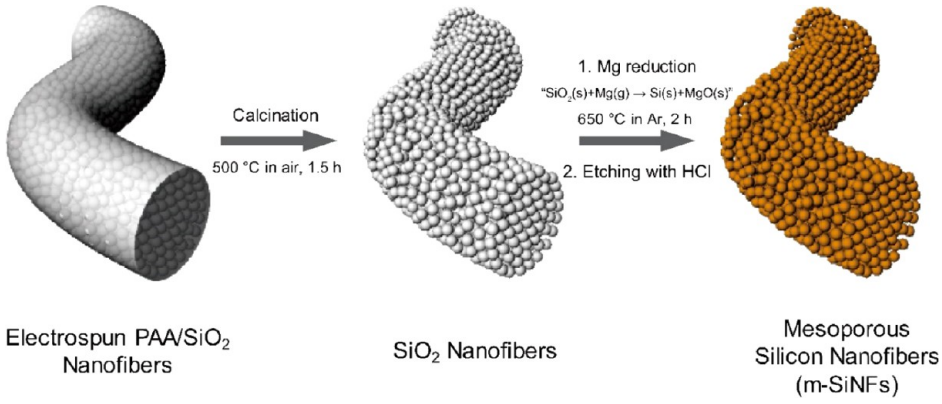

Figure 1. Schematic illustration showing the synthesis of mesoporous silicon nanofibers (m-SiNFs).

chemical performances as anode materials, the complicated process for preparation of silica template or the use of the expensive and toxic precursor, tetraethyl orthosilicate (TEOS),[31] hindered scaling up. Accompanying with an easier and simpler pretreatment step, this method can be an attractive approach to get nanostructured Si anodes. To achieve this goal, here in, we describe a facile and environmentally benign technique for synthesizing mesoporous Si nanofibers (m-SiNFs) using an electrospinning method with a combination of a reduction method. Well-ordered colloidal silica nanofibers with aqueous polymer solutions were electrospun, and thereby, the resulting fibers were thermally reduced with Mg powder.

2. EXPERIMENTAL SECTION

Materials. The materials employed, poly(acrylic acid) (PAA) (M_w = 450 000 g mol^{-1}, Aldrich), colloidal SiO_2 (average diameter = 7 nm, Brunauer–Emmett–Teller or BET surface area = 350 m^2 g^{-1}, 30 wt % suspension in water, Aldrich), Mg powder (98%, Aldrich), and hydrochloric acid (Aldrich), were used as received without further purification.

Fabrication of the m-SiNFs. One gram of the colloidal SiO_2 solution was added into a 7.5 wt % aqueous PAA solution, and the mixture was stirred for 2 h at room temperature. The PAA/SiO_2 ratio was fixed at 1:1 by wt %. The resulting viscous solution was loaded into a syringe with a metal nozzle and then electrospun using an electrospinning system (NanoNC). The syringe pumping rate and the voltage applied were controlled to be 1.0 cm^3 h^{-1} and 12 kV, respectively. The spun fibers were collected on the surface of a metal drum rotating at 500 rpm. The PAA in the SiO_2/PAA fibers was removed by calcination at 500 °C for 1.5 h in air. The SiO_2 fibers were then reduced by a magnesiothermic reaction. Specifically, 1 g of the silica fibers and 1 g of the Mg powder were mixed and placed in a tube furnace filled with Ar. The furnace was then heated to 650 °C at a rate of 2 °C min^{-1}; the furnace was maintained at this temperature for 2 h. The MgO formed during the reduction process was removed by etching with HCl for 6 h, and the etched sample was washed several times with water and dried in vacuum at 60 °C overnight.

Characterization of the m-SiNFs. The surface morphologies of the samples were examined using scanning electron microscopy (SEM) (Sirion, FEI). High-resolution transmission electron microscopy (HRTEM) (JEM-2100F, JEOL, 200 kV) was used to determine the interplanar distance of crystalline Si at high magnifications. X-ray diffraction (XRD) analyses (D/MAX-2500, RIGAKU) were performed to examine the crystal structures of the calcined SiO_2 fibers, as well as those of the SiNFs both before and after etching with HCl. The nitrogen adsorption and desorption isotherms of the SiO_2 fibers and the m-SiNFs were attained using the BET method (Micrometrics, ASAP2010) after degassing the samples at 110 °C for 5 h.

Electrochemical Tests. Electrodes were made using the m-SiNFs or SiNPs (the active material), Super P carbon black, and PAA (the binder) in a weight ratio of 60:20:20. The mass loadings of Si were 0.4–0.6 mg cm^{-2}, and the electrode density was controlled to be 0.6 g cm^{-3}. These electrodes were then used in 2032 coin-type half cells, whose potential profiles, cyclabilities, and rates were determined. The 2032 coin-type half cells were assembled in an Ar-filled glovebox and consisted of the active electrodes, which were placed on copper foil, Li metal counter electrodes, and a polypropylene separator (Celgard), which was soaked with the electrolyte (a 1 M solution of $LiPF_6$ in ethylene carbonate/diethyl carbonate or EC/DEC (50/50 by vol %) containing 5 wt % fluoroethylene carbonate, PANAX ETEC). The assembled cells were cycled at current rates ranging from 100 mA g^{-1} to 80 A g^{-1} over potentials of 0.005–1.5 V (vs Li/Li$^+$) using a WBCS 3000 battery tester (Wonatech) at 25 °C.

3. RESULTS AND DISCUSSIONS

Figure 1 shows the scheme for the fabrication steps as well as the proposed morphologies of the corresponding steps. Electrospinning is an effective, simple, and scalable method for obtaining nanostructures including polymeric,[32] inorganic,[33] and composite[34] one-dimensional (1D) nanofibers and three-dimensional (3D) porous nanofibers for various types of energy devices.[35,36] An aqueous solution containing polyacrylic acid (PAA) and colloidal silica nanoparticles was electrospun to form submicrometer-sized SiO_2 fibers, which had the appearance of the strands of a nonwoven mat (Figure S1a, Supporting Information). The water-soluble PAA polymer acts as a template material and homogeneously blends with the colloidal silica nanoparticles. This polymer template is then removed thermally by heating the fibers at 500 °C for 1.5 h; the process does not affect the morphology of the fibers (Figure S1b, Supporting Information).[37] Then, the prepared SiO_2 nanofibers are mixed with Mg powder and heated up to 650 °C for 2 h in an argon flow, producing Si and MgO. Finally, the reduced MgO is removed by etching with a hydrochloric acid solution (Figure S1c, Supporting Information).[38] Using this procedure, we could fabricate 3D mesoporous silicon nanofibers (m-SiNFs). Well-ordered colloidal silica was chosen as the silicon source because of its small size and large surface area (average particle size ≈ 7 nm; surface area ≈ 350 m^2 g^{-1}); these readily allow magnesium gases to penetrate into the fibers, resulting in the magnesiothermic reaction to form Si nanocrystals with no byproducts, such as Mg_2Si and Mg_2SiO_4, being produced.[38] The prepared m-SiNFs have a unique structure: the primary Si nanoparticles interconnect and form secondary 3D mesoporous nanofibers. Although the nanosized primary particles lead to rapid electronic and ionic diffusion,[17,21,25] the structure of the secondary nanofibers (a few micrometers in length) permits the uniform distribution of nanoparticles, thus

allowing for the easy fabrication of electrodes; these issues have been the main barriers to the commercialization of LIBs based on nanostructured Si materials.[24,25]

The morphologies of the as-prepared electrospun PAA/SiO_2, calcined SiO_2, and reduced Si nanofibers were confirmed using field emission scanning electron microscopy (FESEM), transmission electron microscopy (TEM), and high-resolution TEM (HRTEM) (Figure 2). The morphologies of the electrospun

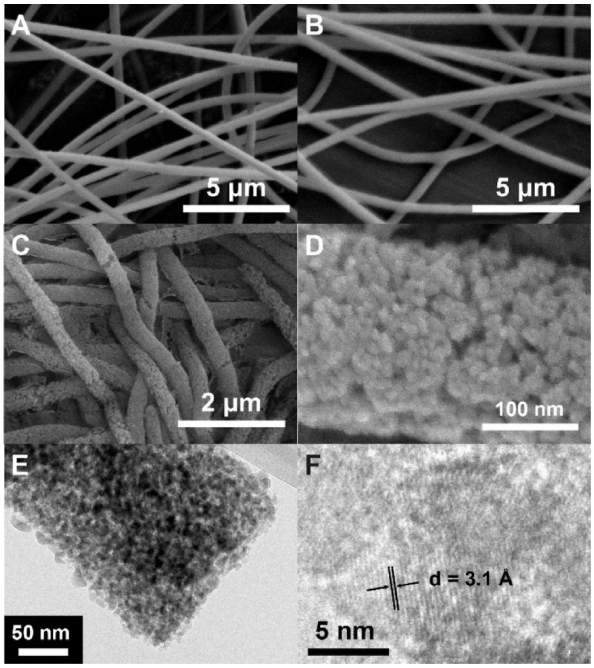

Figure 2. SEM images of the (a) electrospun PAA/SiO_2 nanofibers, (b) SiO_2 nanofibers after being calcined, and (c) and (d) m-SiNFs after the Mg reduction and HCl etching processes. TEM images of (e) an m-SiNF and (f) an HRTEM image of an m-SiNF.

PAA/SiO_2 and calcined SiO_2 nanofibers were almost similar, and they had a diameter of approximately 200 nm. The Si nanofibers formed after the completion of the magnesiothermic reaction, and the etching process also had a similar morphology and diameter; the only exception was that the size of their pores was greater than that of the parent SiO_2 nanofibers (Figure 2e). As can be seen from a HRTEM image (Figure 2f) of an m-SiNF, the interplanar distance was approximately 0.31 nm; this corresponded to the crystalline Si (111) plane.[26] In addition, the Si of the m-SiNFs was identified to be purely crystalline in nature. The crystal structure of the synthesized m-SiNFs was further studied using powder X-ray diffraction (XRD) analysis. Figure 3a shows the XRD patterns of the as-prepared calcined SiO_2, magnesiothermically reduced Si, and chemically etched Si nanofibers. The XRD pattern for the calcined SiO_2 nanofibers exhibited a broad peak at approximately 23°; this was indicative of the presence of an amorphous phase of SiO_2. After the Mg-based reduction reaction, peaks attributable to MgO (JCPDS, No. 00-045-0946) and Si (JCPDS, No. 00-027-1402) were detected, and the broad SiO_2 peak disappeared from the XRD spectrum, indicating that all of the SiO_2 was effectively reduced to Si. The pattern for the prepared m-SiNFs exhibited diffraction peaks at 28.3°, 47.2°, 56.1°, 69.2°, and 76.5°, which corresponded to the (111), (220), (311), (400), and (331) lattice orientations of Si crystals,[39,40] respectively. These results suggested that the synthesized m-SiNFs were free of

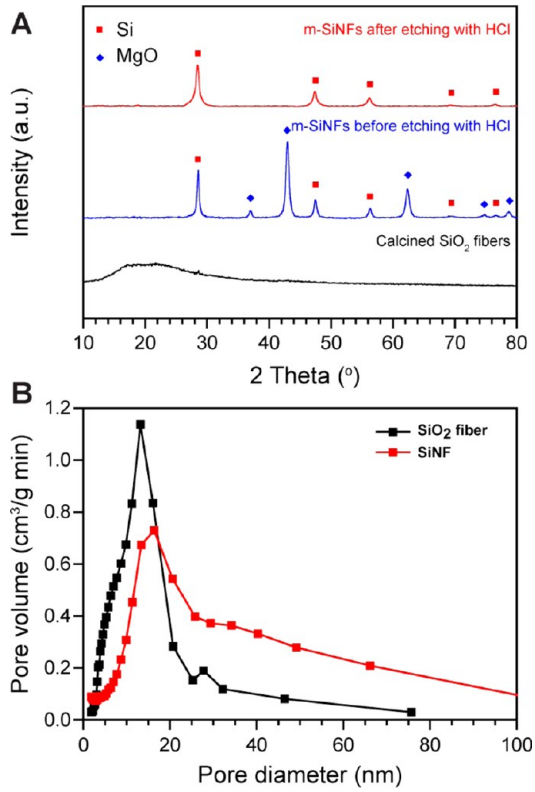

Figure 3. (a) XRD pattern of the calcined SiO_2 nanofibers and those of the m-SiNFs before and after being etched with HCl. (b) BJH pore diameter distributions of the calcined SiO_2 nanofibers and the m-SiNFs after etching with HCl.

impurities such as Mg_2Si or Mg_2SiO_4, which are hard to remove by etching with HCl. Previous studies have reported that these impurities are inevitably produced when vaporized Mg cannot adequately infiltrate into the nanofibers.[38] This clearly indicates that our method provides colloidal silica nanoparticles with well-ordered large surface area porous structures and enables vaporized Mg to infiltrate readily. As a result, no undesirable byproducts, such as Mg_2Si and Mg_2SiO_4, are produced.

Further investigation of the pore structure of calcined SiO_2 nanofibers and the m-SiNFs etched with HCl were conducted using nitrogen adsorption/desorption isotherms (Figure S2, Supporting Information) and Barrett–Joyner–Halenda (BJH) pore diameter distributions (Figure 3b). The isotherms of both types of fibers exhibited hysteresis at high relative pressures, and this reflects the evidence of their mesoporous structures.[41] The specific surface areas of the porous calcined SiO_2 nanofibers and the m-SiNFs were 202.6 and 160.3 $m^2\ g^{-1}$, respectively. In addition, the pore size distributions of the nanofibers, determined via BJH analyses suggested that the average pore diameters of the SiO_2 nanofibers and the m-SiNFs were 9.14 and 12.95 nm, respectively. Higher surface areas of the m-SiNFs (and their pore diameters were lower) compared to that of the SiO_2 nanofibers ascribes to the changes in their pore structure caused by the Mg reduction and MgO etching processes.[39] The presence of mesopores in the anodes of LIBs may allow for easier penetration of the electrolyte, thus improving accessibility for the Li^+ ions. Such anodes can also accommodate the severe volume changes during battery operations.[42] Therefore, m-SiNFs with a 3D mesoporous and interconnected structure can be expected to show desirable electrochemical properties as anode materials for LIBs.

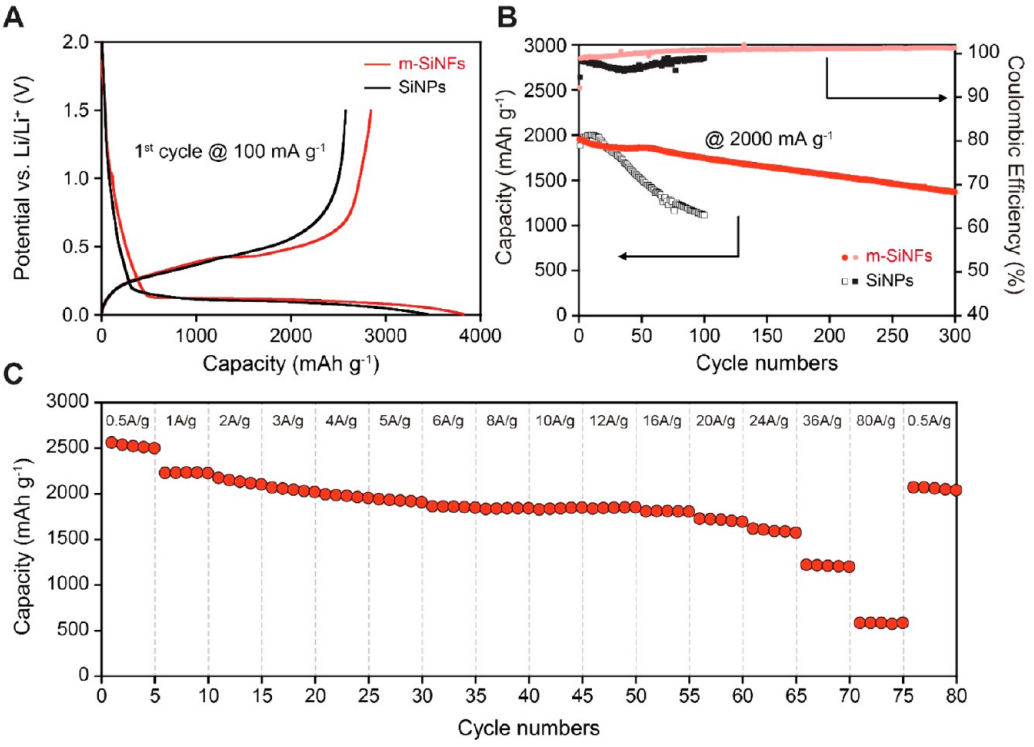

Figure 4. (a) Potential profiles of unit cells fabricated using SiNPs and the m-SiNFs during the first cycle at 0.1 A g^{-1}, (b) cycling performances and coulombic efficiencies of the unit cells fabricated using SiNPs and the m-SiNFs at 2 A g^{-1}, and (c) rate capability of the m-SiNF electrode measured at a series of current rates.

The electrochemical performance of the m-SiNFs was investigated using 2032 coin-type half cells, which employed counter electrodes made of Li metal. In addition, for the purpose of further elucidating the effect of the mesoporous structure of the m-SiNFs on their performance, pore-free anodes of commercial silicon nanoparticles (SiNPs) (particles <100 nm in diameter), the morphologies of these anodes were also confirmed using scanning electron microscopy (SEM) and TEM (Figure S3, Supporting Information), were also prepared and evaluated under the same conditions. The potential profiles of the unit cells fabricated using the m-SiNFs and SiNPs are shown in Figure 4a; these were determined at a current rate of C/20 (100 mA g^{-1}) over voltages ranging from 0.005 to 1.5 V (vs Li/Li^+). Both cell types (m-SiNFs and SiNPs) exhibited characteristic plateaus associated with the lithiation and delithiation of crystalline Si at ~0.1 and ~0.4 V, respectively. These were consistent with the results of previous studies on Si-based anode materials.[20,21] The initial discharge capacities were 2846.7 and 2576.9 mAh g^{-1} for the cells based on the m-SiNFs and SiNPs, respectively; the corresponding initial coulombic efficiencies (ICE) were 74.5 and 74.9%, respectively. An interesting point to note is that the ICE of the unit cell based on the m-SiNFs was very similar to that of the cell based on SiNPs; this implies the absence of byproducts such as Mg_2SiO_4 and residual SiO_2 in the m-SiNFs. Previous studies have reported ICEs of only approximately 60% for mesoporous Si materials obtained from magnesiothermic reduction processes.[38,39] This was because the byproducts and the residual SiO_2 remained within the mesoporous Si nanostructures and irreversibly reacted with Li^+ ions during the first charging process.[43] Moreover, the reversible capacity of the unit cell based on the m-SiNFs was higher than that of the cell based on SiNPs, which is attributed to the unique 3D mesoporous structure of the m-SiNFs that allows for efficient lithiation and delithiation,[25] even at low current densities.

In addition, the cell based on the m-SiNFs exhibited superior cycling performance compared to that of the cell based on SiNPs at 1 C rate (2000 mA g^{-1}) (Figure 4b). The unit cell based on SiNPs exhibited rapid capacity fading after 100 cycles (59.1% of its initial capacity, which was 1125.4 mAh g^{-1}), and its average coulombic efficiency (CE) was 94.6%. These results indicate that commercial SiNPs do not exhibit sufficiently high cyclability as an anode material for LIBs. It is likely that the absence of voids in the electrodes fabricated from SiNPs causes a loss in electrical contact among the particles. This, in addition to the pulverization of the SiNPs, is the main cause of the inferior capacity retention and poor CE.[17] In contrast, the cells based on the m-SiNFs exhibited a discharge capacity of approximately 2000 mAh g^{-1}, retaining 89.4% of its initial discharge capacity after 100 cycles and 70.0% after 300 cycles (1363.4 mAh g^{-1}). The reversible volumetric capacity of the m-SiNFs was 1200 mAh cm^3, which is approximately 2.4 times larger than that of commercial graphitic carbon anodes (ca. 500 mAh cm^3). The electrode density of the m-SiNFs is 0.6 g cm^{-3} (mass loading of m-SiNFs, 0.6 mg cm^{-2}; electrode thickness, 10 μm). Moreover, its average CE was 99.8% for up to 100 cycles; this value was comparable to those of commercial graphitic carbons.

The cells based on the m-SiNFs also exhibited excellent rate capabilities for current densities ranging from 0.5 to 80 A g^{-1} (Figures 4c and S4 (Supporting Information)). Even when the current rate was increased 72-fold, from 0.5 to 36 A g^{-1}, the rate capability of the cells remained as high as 1214.0 mAh g^{-1} for a discharge time as short as ~3 min. In addition, as the current density was lowered to 0.5 A g^{-1}, the cells recovered 80.8% of its original capacity (2064.0 mAh g^{-1}). Because

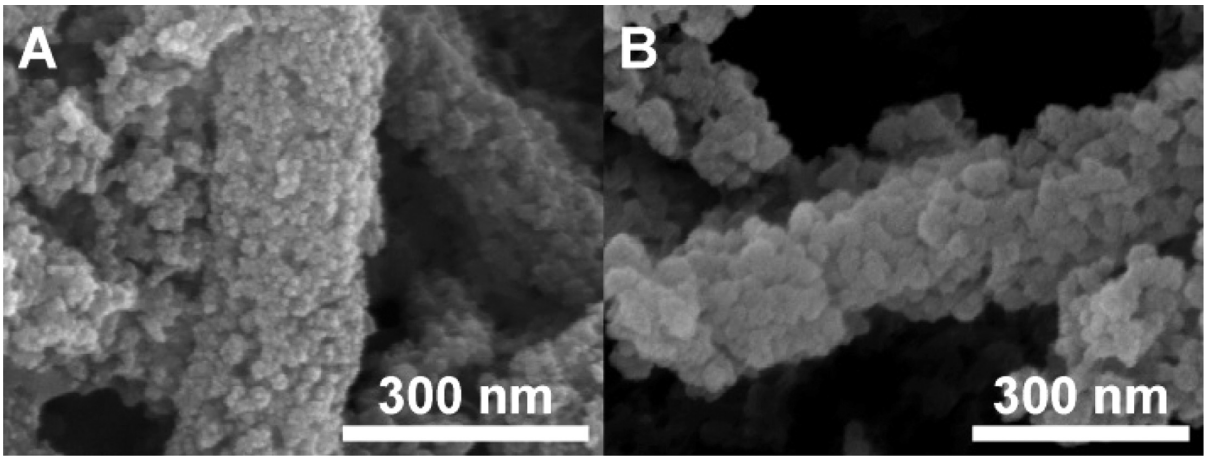

Figure 5. SEM images of the m-SiNF electrode (a) before cycling and (b) after 300 cycles.

loading mass plays a crucial role in determining cell performances and rate capabilities of the unit cells, it was not possible to precisely compare the cell performances of each group. However, compared with various Si anode materials introduced in previous studies, the m-SiNFs are not only easily synthesized via scalable method but also show excellent rate capability (Table S1, Supporting Information). The superior electrochemical characteristics including high reversible capacity, capacity retention, CE during cycling, and rate capability, exhibited by the unit cells based on the m-SiNFs are evidence of the positive effects of the mesoporous and bicontinuous structure composed of nanosized primary Si particles of the synthesized m-SiNFs on LIB performance.

Finally, to determine whether the morphology of the m-SiNFs was preserved after battery cycling, the cells based on the m-SiNFs were disassembled, and the anode was examined (Figure 5). The SEM images of the anode indicated that the overall fibrous structure of the m-SiNFs remained unaffected; however, the diameter of the fibers increased from 250 to 350 nm, owing to the change in the volume of the fibers during repeated cycling. This stability of the morphology indicated that the porous m-SiNFs allowed excellent pathways for the electrolyte in spite of the large changes in their volume.

4. CONCLUSION

In summary, we successfully prepared 3D mesoporous silicon nanofibers using a simple technique involving electrospinning and the magnesiothermic reduction of silica. These m-SiNFs exhibited highly desirable electrochemical characteristics for use as an anode material for LIBs. The cells fabricated using these m-SiNFs showed a reversible capacity as high as 2846.7 mAh g^{-1} at a current density of 0.1 A g^{-1}. It also exhibited a stable capacity retention of 89.4% at a 1 C rate (2 A g^{-1}) over 100 cycles and a rate capability of up to 36 A g^{-1} (1214.0 mAh g^{-1}). These electrochemical properties of the m-SiNFs can be attributed to the fact that their constituent Si nanoparticles form mesoporous and interconnected nanostructures that permit the fibers to not only accommodate large changes in volume during battery operation but also allow Li^+ ion greater access. Moreover, given the scalable and facile nature of the synthesis procedure, these m-SiNFs can be exploited commercially as an anode material for LIBs.

■ ASSOCIATED CONTENT

Ⓢ Supporting Information

Photographs of nanofibers, nitrogen adsorption/desorption isotherms, SEM and TEM images of Si nanoparticles, potential profiles of the m-SiNF electrode measured at a series of current rates, and summary of previous studies on rate performance of various Si anode materials. This material is available free of charge via the Internet at http://pubs.acs.org.

■ AUTHOR INFORMATION

Corresponding Authors

*Y. M. Lee. E-mail: yongmin.lee@hanbat.ac.kr.
*J.-K. Park. E-mail:jungpark@kaist.ac.kr.

Notes

The authors declare no competing financial interest.

■ ACKNOWLEDGMENTS

This research was supported by the National Research Foundation of Korea Grant funded by the Korean Government (MEST) (NRF-2010-0029031).

■ REFERENCES

(1) Tarascon, J. M.; Armand, M. *Nature* **2001**, *414* (6861), 359−367.
(2) Aricò, A. S.; Bruce, P.; Scrosati, B.; Tarascon, J. M.; Van Schalkwijk, W. *Nat. Mater.* **2005**, *4* (5), 366−377.
(3) Besenhard, J. O.; Winter, M. *ChemPhysChem* **2002**, *3* (2), 155−159.
(4) Armand, M.; Tarascon, J. M. *Nature* **2008**, *451* (7179), 652−657.
(5) Etacheri, V.; Marom, R.; Elazari, R.; Salitra, G.; Aurbach, D. *Energy Environ. Sci.* **2011**, *4* (9), 3243−3262.
(6) Liu, C.; Li, F.; Lai-Peng, M.; Cheng, H. M. *Adv. Mater.* **2010**, *22* (8), E28−E62.
(7) Dunn, B.; Kamath, H.; Tarascon, J. M. *Science* **2011**, *334* (6058), 928−935.
(8) Scrosati, B.; Garche, J. *J. Power Sources* **2010**, *195* (9), 2419−2430.
(9) Li, H.; Wang, Z.; Chen, L.; Huang, X. *Adv. Mater.* **2009**, *21* (45), 4593−4607.
(10) Dahn, J. R.; Zheng, T.; Liu, Y.; Xue, J. S. *Science* **1995**, *270* (5236), 590−598.
(11) Flandrois, S.; Simon, B. *Carbon* **1999**, *37* (2), 165−180.
(12) Palacín, M. R. *Chem. Soc. Rev.* **2009**, *38* (9), 2565−2575.
(13) Fauteux, D.; Koksbang, R. *J. Appl. Electrochem.* **1993**, *23* (1), 1−10.
(14) Jeong, G.; Kim, Y. U.; Kim, H.; Kim, Y. J.; Sohn, H. J. *Energy Environ. Sci.* **2011**, *4* (6), 1986−2002.

(15) Kasavajjula, U.; Wang, C.; Appleby, A. J. *J. Power Sources* **2007**, *163* (2), 1003−1039.
(16) Szczech, J. R.; Jin, S. *Energy Environ. Sci.* **2011**, *4* (1), 56−72.
(17) Wu, H.; Cui, Y. *Nano Today* **2012**, *7* (5), 414−429.
(18) Lee, Y. M.; Lee, J. Y.; Shim, H. T.; Lee, J. K.; Park, J. K. *J. Electrochem. Soc.* **2007**, *154* (6), A515−A519.
(19) Zhang, W. J. *J. Power Sources* **2011**, *196* (1), 13−24.
(20) Ryu, J. H.; Kim, J. W.; Sung, Y. E.; Oh, S. M. *Electrochem. Solid-State Lett.* **2004**, *7* (10), A306−A309.
(21) Chan, C. K.; Peng, H.; Liu, G.; McIlwrath, K.; Zhang, X. F.; Huggins, R. A.; Cui, Y. *Nat. Nanotechnol.* **2008**, *3* (1), 31−35.
(22) Yao, Y.; McDowell, M. T.; Ryu, I.; Wu, H.; Liu, N.; Hu, L.; Nix, W. D.; Cui, Y. *Nano Lett.* **2011**, *11* (7), 2949−2954.
(23) Song, T.; Xia, J.; Lee, J. H.; Lee, D. H.; Kwon, M. S.; Choi, J. M.; Wu, J.; Doo, S. K.; Chang, H.; Park, W. I.; Zang, D. S.; Kim, H.; Huang, Y.; Hwang, K. C.; Rogers, J. A.; Paik, U. *Nano Lett.* **2010**, *10* (5), 1710−1716.
(24) Lee, K. T.; Cho, J. *Nano Today* **2011**, *6* (1), 28−41.
(25) Guo, Y. G.; Hu, J. S.; Wan, L. J. *Adv. Mater.* **2008**, *20* (23), 2878−2887.
(26) Bao, Z.; Weatherspoon, M. R.; Shian, S.; Cai, Y.; Graham, P. D.; Allan, S. M.; Ahmad, G.; Dickerson, M. B.; Church, B. C.; Kang, Z.; Abernathy Iii, H. W.; Summers, C. J.; Liu, M.; Sandhage, K. H. *Nature* **2007**, *446* (7132), 172−175.
(27) Jia, H.; Gao, P.; Yang, J.; Wang, J.; Nuli, Y.; Yang, Z. *Adv. Energy Mater.* **2011**, *1* (6), 1036−1039.
(28) Chen, D.; Mei, X.; Ji, G.; Lu, M.; Xie, J.; Lu, J.; Lee, J. Y. *Angew. Chem., Int. Ed.* **2012**, *51* (10), 2409−2413.
(29) Yoo, J. K.; Kim, J.; Jung, Y. S.; Kang, K. *Adv. Mater.* **2012**, *24* (40), 5452−5456.
(30) Yoo, J. K.; Kim, J.; Lee, H.; Choi, J.; Choi, M. J.; Sim, D. M.; Jung, Y. S.; Kang, K. *Nanotechnology* 2013, *24*, (42), in press.
(31) Ito, T.; Matumoto, T.; Nishioka, K. *Surf. Coat. Technol.* **2013**, *215* (0), 447−451.
(32) Choi, S. W.; Jo, S. M.; Lee, W. S.; Kim, Y. R. *Adv. Mater.* **2003**, *15* (23), 2027−2032.
(33) Mai, L.; Xu, L.; Han, C.; Xu, X.; Luo, Y.; Zhao, S.; Zhao, Y. *Nano Lett.* **2010**, *10* (11), 4750−4755.
(34) Raghavan, P.; Zhao, X.; Kim, J. K.; Manuel, J.; Chauhan, G. S.; Ahn, J. H.; Nah, C. *Electrochim. Acta* **2008**, *54* (2), 228−234.
(35) Thavasi, V.; Singh, G.; Ramakrishna, S. *Energy Environ. Sci.* **2008**, *1* (2), 205−221.
(36) Cavaliere, S.; Subianto, S.; Savych, I.; Jones, D. J.; Rozière, J. *Energy Environ. Sci.* **2011**, *4* (12), 4761−4785.
(37) Horzum, N.; Muñoz-Espí, R.; Glasser, G.; Demir, M. M.; Landfester, K.; Crespy, D. *ACS Appl. Mater. Interfaces* **2012**, *4* (11), 6338−6345.
(38) Chen, W.; Fan, Z.; Dhanabalan, A.; Chen, C.; Wang, C. *J. Electrochem. Soc.* **2011**, *158* (9), A1055−A1059.
(39) Tao, H. C.; Fan, L. Z.; Qu, X. *Electrochim. Acta* **2012**, *71*, 194−200.
(40) Yu, Y.; Gu, L.; Zhu, C.; Tsukimoto, S.; Van Aken, P. A.; Maier, J. *Adv. Mater.* **2010**, *22* (20), 2247−2250.
(41) Sing, K. S. W.; Everett, D. H.; Haul, R. A. W.; Moscou, L.; Pierotti, R. A.; Rouquerol, J.; Siemieniewska, T. *Pure Appl. Chem.* **1985**, *57* (4), 603−619.
(42) Kim, H.; Cho, J. *Nano Lett.* **2008**, *8* (11), 3688−3691.
(43) Yang, J.; Takeda, Y.; Imanishi, N.; Capiglia, C.; Xie, J. Y.; Yamamoto, O. *Solid State Ionics* **2002**, *152-153*, 125−129.